Mon. Not. R. Astron. Soc. **000**, 1–10 (2005) Printed 5 January 2014 (MN LATEX style file v2.2)

Circumstellar discs in the young σ Orionis cluster

J.M. Oliveira⋆, R.D. Jeffries, J.Th. van Loon and M.T. Rushton
School of Physical and Geographical Sciences, Lennard-Jones Laboratories, Keele University, Keele, Staffordshire ST5 5BG, UK

ABSTRACT

We present new K- and L′-band imaging observations for members of the young (3−5 Myr) σ Orionis cluster, obtained with UIST at UKIRT. We determine $(K - L')$ colour excesses with respect to the photospheres, finding evidence for warm circumstellar dust around 27 out of 83 cluster members that have masses between $0.04\,M_\odot$ and $1.0\,M_\odot$. This indicates a circumstellar disc frequency of at least $(33 \pm 6)\%$ for this cluster, consistent with previous determinations from smaller samples (Oliveira, Jeffries & van Loon 2004) and also consistent with the 3 Myr disc half-life suggested by Haisch, Lada & Lada (2001b). There is marginal evidence that the disc frequency declines towards lower masses, but the data are also consistent with no mass-dependence at all. There is no evidence for spatial segregation of objects with and without circumstellar discs.

Key words: circumstellar matter – infrared: stars – stars: pre-main-sequence – stars: low-mass, brown dwarfs – open clusters and associations: individual (σ Orionis)

1 INTRODUCTION

Circumstellar discs play an important role in the formation and early evolution of low-mass stars. There is ample empirical evidence that the majority of stars are born with circumstellar discs (Haisch, Lada & Lada 2000; Lada et al. 2000). It has also become clear that dust discs are removed relatively quickly, likely within 10 Myr (Haisch, Lada & Lada 2001b). As the building blocks for planetary systems, it is imperative that we understand disc processes. In particular the timescale for disc dissipation is crucial in determining whether planets form and on what timescales (Brandner et al. 2000) and might control exoplanet growth and migration (Lecar & Sasselov 2003). It is also not well understood how the star formation environment might condition disc evolution and consequently planet formation.

Recently, a huge observational effort has been channelled into determining the disc frequency in star forming regions, in order to empirically constrain the disc destruction timescale. Circumstellar dust discs are cooler than the stellar photospheres, therefore they irradiate mainly at infrared (IR) wavelengths. In particular, a $(K - L)$ colour excess is a robust disc indicator (Wood et al. 2002), at least for the first few Myr; for older associations the inner disc becomes optically thin and dust excesses are only detected at longer wavelengths (Uchida et al. 2004; Megeath et al. 2005). Using $(K - L)$ excess as a disc indicator, Haisch et al. (2001b) determine that within the first 3 Myr approximately half of the dust discs disappear and that at 6 Myr most low-mass stars have lost their discs. This timescale relies on few clusters with rather uncertain ages; observations of more clusters in the crucial 3−5 Myr age range are essential.

The σ Orionis association was first identified in *ROSAT* images as a concentration of bright X-ray sources around the massive multiple system (Wolk 1996). Photometric surveys (Béjar et al. 2001; Sherry, Walter & Wolk 2004) identified a score of pre-main-sequence (PMS) candidates well into the brown dwarf regime and Zapatero Osorio et al. (2000) discovered several objects with masses below the deuterium burning limit (for ongoing surveys on very-low-mass cluster candidates see Caballero 2005). Optical spectroscopy has been used to confirm membership for many cluster candidates (Zapatero Osorio et al. 2002; Barrado y Navascués et al. 2003; Kenyon et al. 2005). Scholz & Eislöffel (2004) investigate variability and rotation in very low-mass cluster members while Franciosini, Pallavicini & Sanz-Forcada (2005) analysed the XMM-*Newton* X-ray properties of PMS stars within the central 30 arcmin area. The age of the cluster is 3−5 Myr (e.g., Zapatero Osorio et al. 2002; Oliveira, Jeffries & van Loon 2004) for an Hipparcos distance (to the central star) of 352 pc. The reddening towards the cluster namesake is low, $E(B - V) = 0.05$ (e.g., Brown et al. 1994).

We have been investigating the IR properties of the σ Ori cluster members. Van Loon & Oliveira (2003) and Oliveira & van Loon (2004) use mid-IR imaging and spectroscopy to confirm several objects as classical T Tauri stars (CTTS) and therefore likely members of the σ Ori cluster. Oliveira et al. (2004) use $(K - L')$ excesses for a sample of 24 cluster members to constrain the cluster disc frequency;

⋆ E-mail: joana@astro.keele.ac.uk

they found that $(46 \pm 14)\%$ of cluster members retain their discs. We have since expanded that thermal-IR survey; we here present new imaging observations of an additional 59 cluster members in the K- and L′-bands. We compute the disc frequency for the complete sample of 83 cluster members and investigate the mass dependence of disc dissipation across a wider mass range.

2 SAMPLE OF CLUSTER MEMBERS

Targets were selected from several samples from the literature. Objects from Zapatero Osorio et al. (2002), Barrado y Navascués et al. (2003), Muzerolle et al. (2003) and Kenyon et al. (2005) have been confirmed as cluster members using a combination of spectroscopic indicators: the presence of the Li I 6708 Å line, a weak Na I IR doublet and radial velocity measurements. We did not choose members identified on the basis of strong Hα emission in order not to bias the sample towards objects with accretion discs. To complement the sample at the higher mass end we selected high photometric probability ($> 70\,\%$) members from the optical and near-IR sample of Sherry et al. (2004). There are also 2 targets from the photometric sample of Béjar et al. (2001).

Fig. 1 shows the $I/(I-J)$ colour-magnitude diagram of the observed sample as well as the sample from Oliveira et al. (2004), together with isochrones and evolutionary tracks from Baraffe et al. (1998), adopting the Hipparcos distance of 352 pc. Oliveira et al. (2004) investigated whether differential reddening should be taken into account; they found that the only objects to exhibit significant reddening also display an IR excess. We could use the reddening determination towards σ Ori itself, but it is rather small ($E(B-V) = 0.05$, Brown et al. 1994) in particular at IR wavelengths; therefore we follow Oliveira et al. (2004) and do not de-redden targets' magnitudes and colours. The masses of the cluster members are then in the range $0.04-1.0\,M_{\odot}$, with 6 objects below the brown dwarf boundary. The median age of the sample is 4.2 Myr, consistent with previous determinations, e.g., $4.2^{+2.7}_{-1.5}$ Myr from Oliveira et al. (2002). If a larger distance of 440 pc is adopted, the isochronal age of the cluster decreases to 2.5 Myr (Sherry et al. 2004) — and the computed PMS masses are only slightly increased. In any of these studies the presence of hitherto unidentified binaries can cause the age determination to be biased towards younger ages. A small average reddening would also cause the cluster to appear younger, but in the case of the σ Ori cluster this effect is negligible. From the absence of lithium depletion in the cluster members, Zapatero Osorio et al. (2002) estimate an upper limit to the cluster age of 8 Myr. Cluster members also appear to present a large age spread (see discussions in Oliveira et al. 2004 and Burningham et al. 2005). The effect of different age estimates is taken into account later in this discussion.

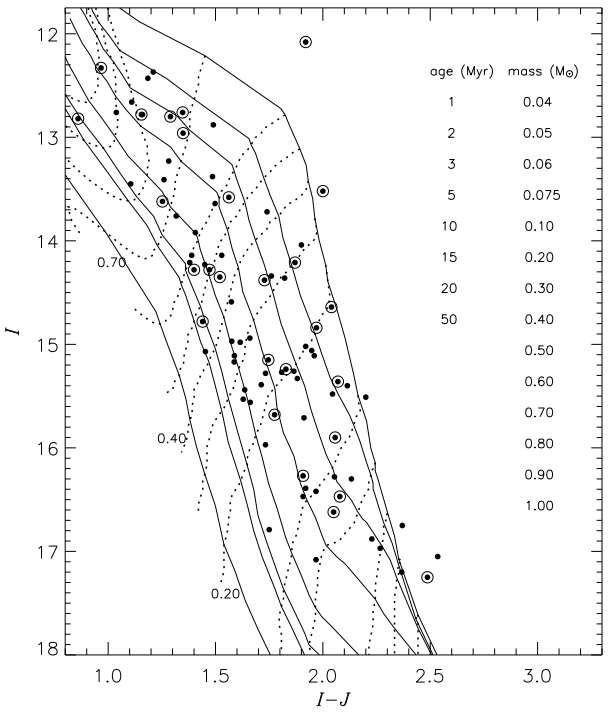

Figure 1. $I/(I-J)$ colour-magnitude diagram of the observed σ Ori cluster members, from Oliveira et al. (2004) and new observations; double-circle objects exhibit a 2-σ $(K-L')$ excess (see Sect. 4.1). Isochrones and evolutionary tracks are from Baraffe et al. (1998) and the Hipparcos distance of 352 pc is used. No extinction correction is performed (see text).

3 OBSERVATIONS: K AND L′-BAND IMAGING

The K- and L′-band imaging was performed with the imager spectrometer UIST at the United Kingdom Infrared Telescope (UKIRT) over semesters 2003B and 2005A. These observations closely follow the strategy described in Oliveira et al. (2004) therefore we just summarise the few major points.

K_s-band magnitudes from 2MASS (Two Micron All Sky Survey, Cutri et al. 2003) were used to set the exposure times in this band, while evolutionary models from Baraffe et al. (1998) provided estimates of the L-band photospheric magnitudes of the targets, in the absence of circumstellar emission. Observations were performed under UKIRT flexible scheduling rules, so that conditions were optimal (dry conditions and seeing better than 0.6 arcsec). Total exposure times in the L′-band range from $\sim$2−60 min, while K-band exposures lasted 1 min. To minimise the effects of variability, observations in the two filters were consecutive. Images were reduced and combined using ORAC-DR (the UKIRT data reduction and high level instrument control software) and aperture photometry was performed with GAIA (Graphical Astronomy and Image Analysis Tool), both Starlink packages. Calibration onto the MKO-NIR (Mauna Kea Observatory Near-Infrared) system (Tokunaga, Simons & Vacca 2002) was achieved using photometric standards (Leggett et al. 2003, and also the UKIRT[1]web page): SAO 112626 ($L' = 8.56 \pm 0.01$ mag) and

Table 1. New photometry of σ Ori cluster members. Column 1 is the target number, columns 2 and 3 are the targets' 2MASS positions, column 4 is the I_c magnitude, columns 5−10 are the 2MASS J, H, K_s magnitudes with uncertainties, columns 11−14 are the new MKO-IR K and L' magnitudes with uncertainties and column 15 gives the target identification. Objects with a label S or K, followed by an ID number, were identified respectively by Sherry et al. (2004) or Kenyon et al. (2005). Object IDs like 4771−1097 and r053833−0236 are X-ray sources from Wolk (1996) — see also Zapatero Osorio et al. (2002).

	RA (^{h} ^{m} ^{s})	DEC (^{d} ^{m} ^{s})	I_c (mag)	J (mag)		H (mag)		K_s (mag)		K (mag)		L' (mag)		Identification
1	05 39 39.38	−2 17 04.5	12.96	11.611	0.023	10.714	0.023	10.172	0.024	10.207	0.009	9.193	0.040	S 33
2	05 38 35.87	−2 30 43.3	12.43*	11.245	0.026	10.598	0.023	10.424	0.024	10.429	0.009	10.257	0.029	4771−1097
3	05 38 44.23	−2 40 19.7	12.33*	11.363	0.026	10.688	0.024	10.439	0.024	10.382	0.009	9.651	0.027	4771−1051
4	05 38 39.82	−2 56 46.2	12.76*	11.413	0.027	10.744	0.023	10.439	0.021	10.452	0.009	9.664	0.026	S 145
5	05 38 47.92	−2 37 19.2	13.58	12.018	0.042	11.239	0.046	10.776	0.037	10.945	0.010	10.080	0.026	S 102
6	05 38 53.07	−2 38 53.6	12.78*	11.625	0.026	11.034	0.026	10.828	0.025	10.780	0.010	10.455	0.022	S 166
7	05 37 24.27	−2 19 07.6	12.76	11.722	0.024	11.039	0.024	10.844	0.023	10.846	0.009	10.707	0.070	S 99
8	05 37 51.61	−2 35 25.7	13.38	11.894	0.026	11.172	0.023	10.977	0.022	11.009	0.010	10.796	0.054	S 125
9	05 39 08.53	−2 51 46.6	13.23	11.948	0.024	11.201	0.023	11.028	0.024	10.982	0.010	10.812	0.020	S 61
10	05 38 08.27	−2 35 56.3	13.64	12.142	0.026	11.376	0.023	11.047	0.019	11.265	0.010	10.801	0.024	S 41
11	05 38 34.06	−2 36 37.5	13.72	11.980	0.027	11.330	0.024	11.077	0.027	10.988	0.001	10.612	0.025	r053833−0236
12	05 39 33.79	−2 20 39.9	13.62	12.367	0.026	11.598	0.023	11.429	0.023	11.495	0.010	11.235	0.015	S 138
13	05 36 29.09	−2 35 48.3	13.76*	12.443	0.024	11.689	0.031	11.495	0.023	11.438	0.010	11.429	0.064	S 143
14	05 38 37.94	−2 05 52.4	13.45	12.345	0.027	11.723	0.024	11.502	0.023	11.500	0.010	11.280	0.043	S 168
15	05 38 58.55	−2 15 27.8	13.92	12.514	0.027	11.790	0.024	11.551	0.021	11.570	0.010	11.337	0.096	S 46
16	05 38 36.69	−2 44 13.7	14.36	12.538	0.027	11.891	0.026	11.623	0.028	11.583	0.011	11.264	0.054	S 16
17	05 38 20.50	−2 34 09.0	14.38	12.652	0.026	11.918	0.023	11.648	0.019	11.810	0.010	11.044	0.022	r053820−0234
18	05 39 02.77	−2 29 55.8	14.14	12.611	0.028	12.001	0.024	11.694	0.023	11.657	0.011	11.452	0.088	S 28
19	05 38 18.86	−2 51 38.8	14.28	12.808	0.023	12.039	0.023	11.733	0.021	11.750	0.011	11.137	0.112	S 39
20	05 38 23.65	−3 01 33.2	14.14	12.751	0.023	12.147	0.026	11.908	0.024	11.884	0.011	11.823	0.050	S 38
21	05 37 54.05	−2 44 40.7	14.59	13.016	0.026	12.339	0.026	12.104	0.022	12.058	0.012	12.134	0.200	S 68
22	05 38 50.78	−2 36 26.8	15.06	13.112	0.026	12.445	0.027	12.200	0.025	12.180	0.012	11.800	0.134	K 9
23	05 39 49.45	−2 23 45.9	15.15	13.404	0.030	12.758	0.030	12.438	0.030	12.300	0.013	11.847	0.047	SOri J053949.3−022346
24	05 39 20.97	−2 30 33.5	15.40	13.286	0.027	12.753	0.027	12.438	0.029	12.359	0.013	11.959	0.043	SOri 3
25	05 39 05.24	−2 33 00.6	14.97	13.394	0.028	12.720	0.024	12.462	0.027	12.500	0.016	12.269	0.034	K 5
26	05 38 23.58	−2 20 47.6	15.24	13.412	0.026	12.799	0.029	12.490	0.031	12.452	0.014	11.866	0.077	K 14
27	05 38 44.49	−2 40 30.5	14.98	13.365	0.034	12.724	0.033	12.497	0.035	12.418	0.016	12.095	0.042	K 6
28	05 37 52.11	−2 56 55.2	15.26	13.395	0.028	12.826	0.024	12.515	0.025	12.477	0.017	12.009	0.059	K 15
29	05 39 39.32	−2 32 25.3	15.48	13.435	0.027	12.910	0.023	12.526	0.027	12.497	0.016	12.075	0.030	SOri 4
30	05 38 23.32	−2 44 14.2	15.27	13.462	0.027	12.852	0.023	12.562	0.024	12.550	0.017	12.321	0.025	K 16
31	05 38 47.66	−2 30 37.4	15.33	13.449	0.030	12.847	0.026	12.585	0.025	12.512	0.015	12.152	0.025	SOri 6
32	05 39 01.16	−2 36 38.9	15.11	13.522	0.027	12.895	0.027	12.605	0.027	12.593	0.014	12.236	0.111	K 10
33	05 38 16.10	−2 38 04.9	15.17	13.583	0.027	12.878	0.023	12.612	0.032	12.589	0.017	12.267	0.066	K 12
34	05 36 46.91	−2 33 28.3	15.28	13.547	0.024	12.968	0.030	12.660	0.028	12.604	0.015	12.479	0.031	K 17
35	05 37 15.16	−2 42 01.6	15.07*	13.617	0.029	12.996	0.031	12.776	0.030	12.670	0.015	12.499	0.220	SOri J053715.1−024202
36	05 39 50.57	−2 34 13.7	15.39	13.677	0.030	13.002	0.026	12.732	0.027	12.682	0.015	12.308	0.074	K 20
37	05 38 54.92	−2 28 58.3	15.44	13.804	0.030	13.201	0.026	12.865	0.030	12.916	0.020	12.634	0.086	K 22
38	05 39 08.22	−2 32 28.4	15.71	13.798	0.026	13.254	0.026	12.917	0.029	12.895	0.021	12.590	0.018	SOri 7
39	05 38 50.61	−2 42 42.9	15.90	13.843	0.030	13.246	0.026	12.963	0.038	12.882	0.021	12.291	0.054	K 32
40	05 39 43.00	−2 13 33.3	15.53	13.901	0.027	13.278	0.026	12.990	0.024	13.010	0.041	12.609	0.047	K 25
41	05 37 56.14	−2 09 26.7	15.68	13.905	0.027	13.291	0.027	13.035	0.026	12.945	0.017	12.352	0.100	K 28
42	05 37 50.32	−2 12 24.7	15.56	13.898	0.024	13.305	0.029	13.044	0.024	13.036	0.019	12.540	0.069	K 26
43	05 39 44.51	−2 24 43.2	16.30	14.167	0.029	13.539	0.024	13.150	0.032	13.066	0.021	12.629	0.030	SOri 10
44	05 38 49.29	−2 23 57.6	16.27	14.362	0.027	13.699	0.026	13.197	0.030	13.194	0.024	12.270	0.090	SOri J053849.2−022358
45	05 37 57.46	−2 38 44.4	16.28	14.226	0.030	13.634	0.029	13.285	0.033	13.286	0.027	12.802	0.016	SOri 12
46	05 38 16.99	−2 14 46.3	15.97	14.237	0.027	13.661	0.032	13.346	0.033	13.274	0.027	12.914	0.051	K 33
47	05 38 10.12	−2 54 50.7	16.47	14.391	0.027	13.757	0.032	13.425	0.045	13.405	0.031	12.773	0.023	K 43
48	05 39 37.60	−2 44 30.5	16.75	14.380	0.031	13.819	0.027	13.384	0.034	13.350	0.029	13.450	0.057	SOri 14
49	05 38 48.10	−2 28 53.6	16.39	14.470	0.033	13.840	0.026	13.435	0.036	13.453	0.030	12.915	0.060	SOri 15
50	05 38 47.15	−2 57 55.7	17.05	14.515	0.032	13.935	0.036	13.461	0.044	13.532	0.027	12.812	0.098	K 56
51	05 39 11.40	−2 33 32.8	16.42	14.452	0.034	13.929	0.029	13.571	0.043	13.560	0.026	13.334	0.115	SOri J053911.4−023333
52	05 38 13.31	−2 51 33.0	16.62	14.570	0.034	13.996	0.033	13.636	0.045	13.627	0.029	13.022	0.042	K 48
53	05 38 38.59	−2 41 55.9	16.47	14.562	0.031	13.972	0.030	13.665	0.040	13.647	0.029	13.256	0.018	K 44
54	05 40 32.49	−2 40 59.8	16.97	14.703	0.038	14.065	0.032	13.709	0.049	13.661	0.031	13.271	0.079	K 54
55	05 38 35.36	−2 25 22.2	16.88	14.652	0.033	14.056	0.036	13.764	0.041	13.725	0.035	13.264	0.039	SOri 22
56	05 39 34.33	−2 38 46.9	17.25	14.763	0.032	14.188	0.037	13.787	0.050	13.755	0.034	13.053	0.031	SOri 21
57	05 38 17.42	−2 40 24.3	17.20	14.833	0.031	14.314	0.037	14.093	0.054	13.926	0.043	13.505	0.160	SOri 27
58	05 38 51.00	−2 49 14.0	16.79	15.040	0.039	14.421	0.033	14.159	0.070	14.140	0.048	13.752	0.091	K 50
59	05 37 27.62	−2 57 10.0	17.08	15.122	0.052	14.480	0.065	14.310	0.088	14.224	0.050	13.662	0.240	K 57

[h]

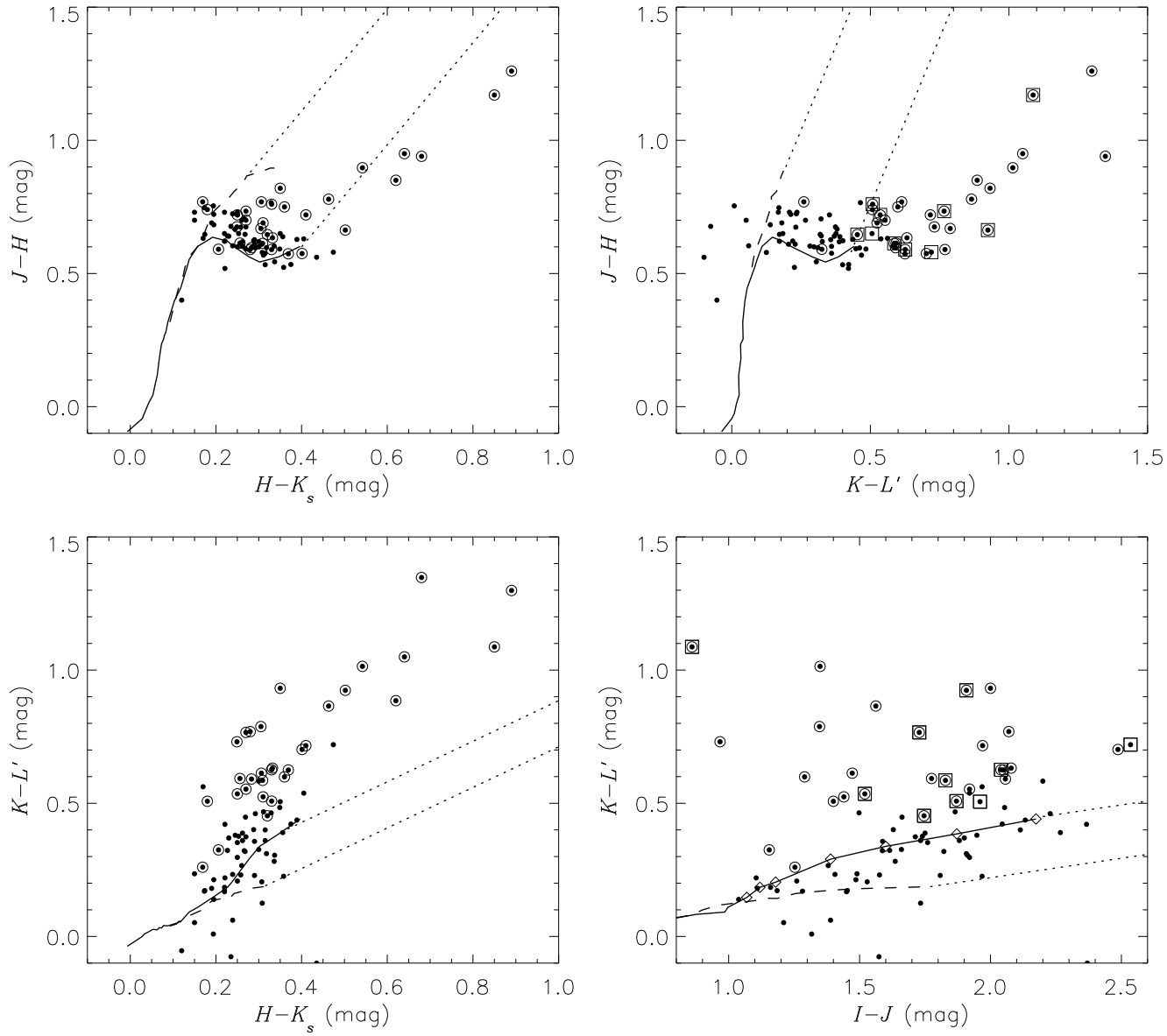

Figure 2. Colour-colour diagrams for the 87 σ Ori cluster members; from left to right and top to bottom: $JHK_{\rm s}$ from 2MASS, $JHKL'$, $HK_{\rm s}KL'$ and $IJKL'$ from 2MASS and our UKIRT observations. The solid and dashed lines are respectively the empirical loci for main-sequence (to spectral type M6) and giant stars and the dotted lines are reddening bands (see text). Double-circle objects have 2-σ $(K-L')$ excess detections. In the $JHKL'$ and $IJKL'$ diagrams we indicate (open squares) objects with Hα equivalent width indicative of stellar accretion (Sect. 5.3). Open diamonds in the $IJKL'$ diagram show the colours of main-sequence stars with spectral types M0−M6.

FS 11 ($K = 11.241 \pm 0.008$ mag), where uncertainties are derived from multiple measurements.

The targets' positions, $I_{\rm c}$ magnitudes, 2MASS J, H and $K_{\rm s}$ photometry, the new K- and L′-band measurements and identifications are listed in Table 1. $I_{\rm c}$ magnitudes are mostly from optical observations described in Kenyon et al. (2005). The 6 objects indicated by * in Table 1 were either saturated or out of their survey area; in these cases we used photometry from Sherry et al. (2004) and Zapatero Osorio et al. (2002). In the analysis described here, we merge the present sample (59 objects) with the sample from Oliveira et al. (2004, 28 objects) as the method for object selection is identical. The total sample thus comprises 87 objects although the 4 known IRAS sources from Oliveira et al. (2004) are excluded from the discussion of the IR excesses and disc frequency, as their selection criteria were different from the remainder of the sample.

[1] http://www.jach.hawaii.edu/UKIRT/astronomy/

4 ANALYSIS OF THE $(K - L')$ COLOURS OF THE CLUSTER MEMBERS

A $(K - L)$ excess in a young star has been proven to be a reliable disc diagnostic (Haisch et al. 2001a; Wood et al. 2002). Determining whether an object has such an excess can be done in two ways: by using colour-colour diagrams, or, if the object's spectral type is known, by directly computing the excess above the photospheric emission.

4.1 Colour-colour diagrams

Fig. 2 shows several colour-colour diagrams for all 87 cluster members. Each diagram shows the object's colours with respect to the loci of main-sequence and giant stars — loci from Bessell & Brett (1988) are converted to the appropriate photometric systems using transformations from Hawarden et al. (2001) and Carpenter (2001). Objects have an excess in $(H - K_s)$ or $(K - L')$ colour when they appear to the right of the reddening band (JHK_s and $JHKL'$ diagrams, top of Fig. 2). Few objects show an excess in $(H-K_s)$, as expected since only accreting discs with high-mass accretion rates have dust warm enough to produce an excess in the K-band (Sect. 5.3). In the $JHKL'$diagram, 33 objects out of the 83 objects appear to the right of the reddening band, indicating a disc frequency of $\sim(40 \pm 7)\%$. Early type objects with small excesses may remain undetected. The computed disc frequency also depends on the adopted spectral type boundary, as noted by Lada et al. (2004). In the next sections we compute $(K - L')$ excesses and identify objects with circumstellar discs, taking into account the corresponding uncertainties.

Fig. 2 (bottom right) also shows the $IJKL'$ colour-colour diagram for the target sample. In this diagram the giant locus (dashed line) sits below the main-sequence locus (solid line). This diagram offers a very clean method of identifying objects with circumstellar discs (i.e. objects that appear above the main-sequence locus) and it is free of some of the problems that affect the usage of other colour-colour diagrams. In particular for late spectral types, the main-sequence locus is for all effects horizontal, meaning that uncertainties in a star's $(I - J)$ colour (e.g., due to accretion variability or stellar activity) do not significantly affect the identification of an $(K - L')$ excess. Furthermore, the effect of reddening is to move a star's position approximately along the same locus, again having a small impact in the disc analysis. This diagram is also more sensitive to early type objects with small excesses and does not depend on any ad hoc spectral-type boundary. Using this diagram, the $(K - L')$ disc frequency for σ Ori cluster members is $\sim(50 \pm 7)\%$, higher than determinations using the $JHKL'$ colour-colour diagram and measured $(K - L')$ excesses (see next section). It is clear that the derived disc frequency is somewhat dependent on the method used.

4.2 $(K - L')$ excesses

We can compute $(K - L')$ excesses individually for each young star if spectral types are known or can estimated. As it can be seen from Table 2, spectral types are only known for a small fraction of the observed sample. Following Oliveira et al. (2004), for objects without published spectral types, we estimate these from the observed colours. We use tabulated relations between colours and spectral type from Bessell & Brett (1988), converted to the appropriate photometric system. We estimate the spectral type that corresponds respectively to the observed $(I - J)$ and $(H - K_s)$ colours — for objects with no obvious $(H - K_s)$ excess, Sect. 5.3. These two quantities are then averaged to compute the values listed in Table 2 (indicated by †). These spectral type determinations are uncertain by about a subclass (see Oliveira et al. 2004, for a full discussion); spectral types measured from optical spectroscopy typically have quoted uncertainties of half a subclass. Accordingly, the excess error listed in the table combines in quadrature the photometric errors with this spectral type error. Fig. 3 shows the spectral types (both estimated and known from the literature) for the sample, plotted against I-band magnitude. A similar diagram (effectively a colour-magnitude diagram) can be found in Barrado y Navascués et al. (2003). For each spectral type, the "scatter" in magnitude is similar between objects with published and estimated spectral types, suggesting reliable spectral type determinations. Both $(I - J)$ and $(H - K_s)$ colours can be affected by the disc itself and interstellar reddening. However, we find good agreement between spectral types computed by this colour method and derived directly from spectroscopy. Furthermore, a mere glance at the $IJKL'$ diagram in Fig. 2 shows that the disc frequency determined in this way is not very sensitive to spectral type (e.g., $(I - J)$) uncertainties (see next paragraph). Therefore we are confident these spectral type determinations are appropriate, *as an aide for the disc frequency determination and as long as spectral type uncertainties are taken into account.*

Of the 83 cluster members in the sample (IRAS sources excluded), 27 objects have 2-σ significant $(K - L')$ excesses, indicating a disc frequency of $(33 \pm 6)\%$. This value is consistent, at the 1-σ level, with $(46 \pm 14)\%$ computed by Oliveira et al. (2004) for a subset of 24 objects (but see Sect. 5.2). These figures are conservative, as we demand a 2-σ significant detection as a disc indicator. Furthermore, for fainter targets increasing L′-band uncertainties mean that we might be unable to detect a small excess. The analysis of the $IJKL'$ diagram in Fig. 2 confirms that all 2-σ detections are reliable and it also suggests that more objects might have a $(K - L')$ excess, just not statistically significant. Thus this disc frequency should be taken as a lower limit.

5 DISCUSSION

5.1 Sample contamination and X-ray luminosities

Most of our sample has supporting spectroscopic evidence of cluster membership (i.e. their spectra show spectroscopic indicators of youth and their radial velocities are consistent with cluster membership, see Sect. 2) but 19 objects are selected only on the basis of their photometry. Because contaminating field stars would be unlikely to have circumstellar emission it is important to assess the level of this contamination and determine its effect on our derived disc frequencies. As young stars are (on average) much more X-ray luminous than any older contaminating field objects (e.g.,

Table 2. IR excesses for the target sample. Column 2 gives the spectral type; † indicates objects with spectral types estimated from their colours. Columns 3, 4 and 5 and 6, 7 and 8 are the measured colours, excesses and uncertainties, respectively for $(H - K_s)$ and $(K - L')$. Column 9 is the Hα equivalent width, EW[Hα]. Column 10 gives references for the spectral type classification and/or EW[Hα]: Zapatero Osorio et al. (2002, ZO02), Barrado y Navascués et al. (2003, B03), Scholz & Eislöffel (2004, SE04) and Muzerolle et al. (2003, M03). "a" in column 9 indicates accreting objects, based on Hα emission line width (Kenyon et al. 2005, K05). Column 11 is the objects' identifications.

	SpT	$(H - K_s)$			$(K - L')$			EW[Hα]	References	Identification
		observed	excess	error	observed	excess	error	(Å)		
1	M3†	0.542	0.265	0.052	1.014	0.724	0.072			S 33
2	K6	0.174	0.026	0.038	0.172	0.071	0.042	2.2	ZO02	4771−1097
3	K7.5	0.249	0.074	0.039	0.731	0.603	0.041	6.4	ZO02	4771−1051
4	M3†	0.305	0.028	0.050	0.788	0.497	0.066			S 145
5	M4†	0.463	0.161	0.071	0.865	0.527	0.066			S 102
6	M1†	0.206	−0.021	0.046	0.345	0.140	0.046			S 166
7	M0†	0.195	0.002	0.044	0.139	−0.007	0.081			S 99
8	M1.5†	0.195	−0.037	0.043	0.213	0.018	0.067			S 125
9	M0.5†	0.173	−0.036	0.044	0.170	0.004	0.045			S 61
10	M4†	0.329	0.027	0.049	0.464	0.125	0.065			S 41
11	M4	0.253	−0.048	0.041	0.376	0.037	0.039	14	ZO02	r053833−0236
12	M0.5†	0.169	−0.040	0.044	0.260	0.094	0.043			S 138
13	M1†	0.194	−0.033	0.048	0.009	−0.175	0.076			S 143
14	M1†	0.221	−0.006	0.044	0.220	0.035	0.059			S 168
15	M2.5†	0.239	−0.018	0.051	0.233	−0.014	0.113			S 46
16	M4†	0.268	−0.033	0.055	0.319	−0.019	0.081			S 16
17	M4	0.270	−0.031	0.035	0.766	0.427	0.038	28	ZO02	r053820−0234
18	M4†	0.307	0.005	0.052	0.205	−0.133	0.107			S 28
19	M3.5†	0.306	0.016	0.050	0.613	0.298	0.127			S 39
20	M2.5†	0.239	−0.018	0.053	0.061	−0.186	0.078			S 38
21	M3†	0.235	−0.042	0.052	−0.076	−0.366	0.209			S 68
22	M4†	0.245	−0.056	0.054	0.380	0.041	0.147			K 9
23	M4	0.320	0.018	0.046	0.453	0.114	0.057	42	ZO02	SOri J053949.3−022346
24	M5†	0.315	−0.031	0.056	0.400	0.014	0.074			SOri 3
25	M3†	0.258	−0.018	0.053	0.231	−0.059	0.070			K 5
26	M4.5†	0.309	−0.015	0.058	0.586	0.224	0.098	a	K05	K 14
27	M2.5†	0.227	−0.030	0.062	0.323	0.075	0.074			K 6
28	M4.5†	0.311	−0.013	0.052	0.468	0.106	0.085			K 15
29	M5.5†	0.375	0.003	0.053	0.422	0.008	0.068			SOri 4
30	M4†	0.290	−0.011	0.052	0.229	−0.109	0.067			K 16
31	M4†	0.262	−0.039	0.053	0.360	0.021	0.066			SOri 6
32	M4†	0.290	−0.011	0.055	0.357	0.018	0.126			K 10
33	M3†	0.266	−0.010	0.056	0.322	0.031	0.090			K 12
34	M4.5†	0.308	−0.016	0.057	0.125	−0.236	0.072			K 17
35	M4	0.220	−0.081	0.047	0.172	−0.166	0.223	4.9	ZO02	SOri J053715.1−024202
36	M3.5†	0.270	−0.019	0.054	0.374	0.053	0.099			K 20
37	M4†	0.336	0.034	0.056	0.282	−0.056	0.106			K 22
38	M5†	0.337	−0.009	0.055	0.305	−0.080	0.066			SOri 7
39	M4†	0.283	−0.018	0.060	0.591	0.252	0.083			K 32
40	M4†	0.288	−0.013	0.053	0.401	0.062	0.086			K 25
41	M3.5†	0.256	−0.033	0.054	0.593	0.278	0.117			K 28
42	M3.5†	0.269	−0.020	0.054	0.448	0.133	0.093			K 26
43	M6†	0.389	−0.007	0.056	0.437	−0.003	0.070			SOri 10
44	M5†	0.502	0.155	0.056	0.924	0.538	0.110	21.3a	SE04, K05	SOri J053849.2−022358
45	M6	0.349	−0.047	0.048	0.484	0.043	0.043	9	M03	SOri 12
46	M4.5†	0.315	−0.009	0.060	0.360	−0.001	0.083			K 33
47	M5†	0.332	−0.014	0.068	0.632	0.246	0.071			K 43
48	M6.5†	0.435	0.013	0.059	−0.100	−0.568	0.087			SOri 14
49	M5.5	0.405	0.033	0.048	0.538	0.124	0.073	15.7	B03	SOri 15
50	M7†	0.474	0.027	0.069	0.720	0.223	0.118	a	K05	K 56
51	M5	0.358	0.011	0.055	0.226	−0.159	0.121	4.7	B03	SOri J053911.4−023333
52	M5.5†	0.369	−0.002	0.068	0.625	0.211	0.078			K 48
53	M5†	0.318	−0.028	0.064	0.311	−0.074	0.069			K 44
54	M5.5†	0.356	−0.015	0.070	0.390	−0.023	0.103			K 54
55	M6	0.292	−0.104	0.058	0.461	0.020	0.060	6.8	B03	SOri 22
56	M6.5†	0.401	−0.020	0.073	0.702	0.233	0.075			SOri 21
57	M7	0.221	−0.225	0.068	0.421	−0.075	0.168	5.1	B03	SOri 27
58	M4.5†	0.262	−0.062	0.087	0.388	0.026	0.119			K 50
59	M5†	0.170	−0.176	0.116	0.562	0.176	0.252			K 57

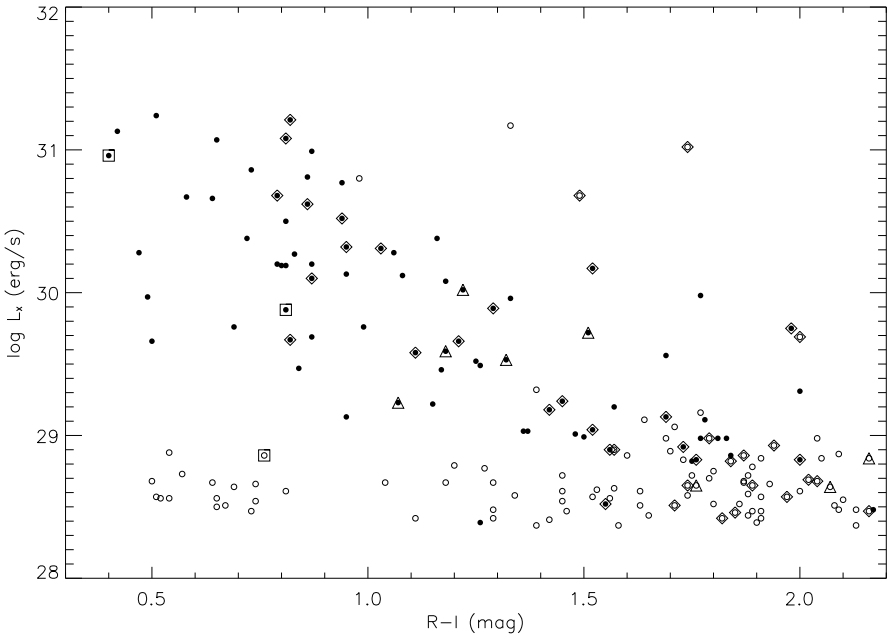

Figure 4. X-ray luminosities for σ Ori cluster members and candidates from Franciosini et al. (2005). Filled circles are XMM-*Newton* detections and open circles are 3-σ upper limits (see their Tables A1 and A2). Also plotted are the objects in our sample that fall onto the EPIC field: diamonds are spectroscopic cluster members, triangles are photometric candidates and squares are IRAS sources (see text).

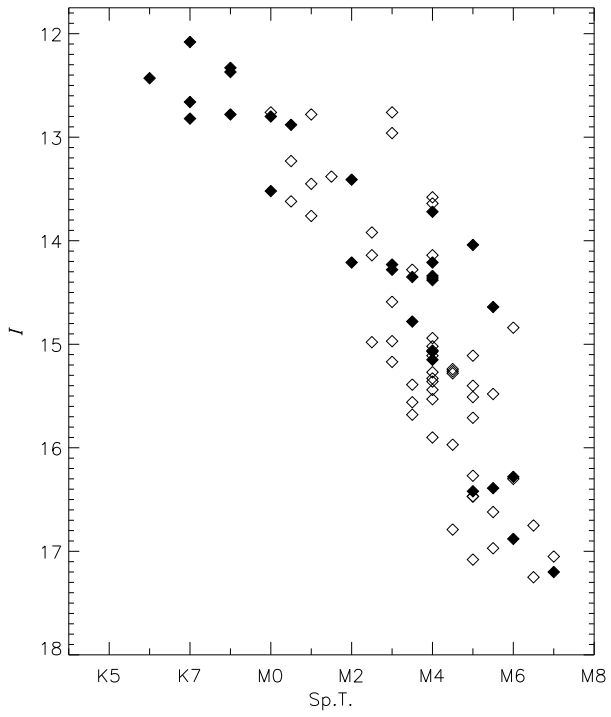

Figure 3. Spectral types versus I-band magnitude for observed cluster members. Filled symbols are objects which have published spectral types, determined from optical spectra, while open symbols represent objects with spectral types determined from observed colours. The scatter in computed spectral types is not significantly larger than the scatter from "classical" spectral typing.

Feigelson et al. 2003), we can use X-ray luminosities as another membership indicator.

Franciosini et al. (2005) have recently analysed XMM-*Newton* observations of an EPIC field centered on the O-star σ Ori (area of diameter $\sim$30 arcmin). From our sample, 51 targets lie within the EPIC field of view. Cross-correlating these targets with the X-ray data we find 30 objects with X-ray detections and 3-σ upper limits for the rest.

The X-ray luminosities are presented as a function of $(R-I)$ colour in Fig. 4. Of the 19 photometric candidates, 8 are in the EPIC field and 5 are detected with X-ray luminosities greater than $10^{29}\,\mathrm{erg\,s^{-1}}$. It is highly unlikely that contaminating field M-dwarfs would have X-ray luminosities as high as this (see Jeffries et al. 2006, and references therein for an analysis of X-ray luminosity evolution with time), and so these 5 young M stars are highly probable cluster members. The 3 non-detections are at colours of $(R-I) > 1.7$ where the lack of an X-ray detection does not adequately discriminate between very young stars and field M-dwarfs because the X-ray survey is not sensitive enough. Indeed, many spectroscopically confirmed members are not detected in X-rays at these colours (Fig. 4). According to Kenyon et al. (2005), almost all objects in photometrically selected cluster samples with $(R-I) > 1.7$ are revealed as genuine cluster members when spectroscopic indicators are used, so we have little doubt that the contamination among these cool photometrically selected candidates is very small.

Even if we were reasonably conservative and use the published photometric membership probabilities of Sherry et al. (2004) — i.e. ignoring the X-ray evidence — we estimate that 17% of the 19 photometric candidates might be contaminants. Even if these $\sim$ 3 objects are assumed not to have discs and are removed from the sample it cannot

raise the deduced disc frequency significantly. Alternatively, we can simply ignore the 11 photometric cluster candidates that lie outside the EPIC field of view and therefore have no supporting X-ray evidence for their membership. The resulting disc frequency is still 32%, consistent with our estimates in the previous section. We have also confirmed that such a procedure would not affect our conclusions regarding any mass dependence of the disc frequency (see next section).

The disc frequency for objects in the EPIC field is (33 ± 8)% while the disc frequency for objects outside this central area is (31 ± 9)%. These estimates are indistinguishable from the total disc frequency of (33 ± 6)%, thus we find no evidence for any spatial segregation of objects with and without circumstellar discs.

5.2 Mass dependence of disc frequency

One of the main goals behind the σ Ori cluster survey was to investigate the possibility of a mass dependence in the disc frequency. Using the colour-magnitude diagram and isochrones from Fig. 1, we have determined the masses and ages of the cluster members. We have divided the sample in 3 mass bins and determined the disc frequency in each bin. The mass bins are $M \geqslant 0.5\,M_\odot$, $0.5\,M_\odot > M \geqslant 0.1\,M_\odot$ and $0.1\,M_\odot > M \geqslant 0.04\,M_\odot$; the respective disc frequencies are 11/26 or (42 ± 13)%, 13/45 or (28 ± 8)% and 3/12 or (25 ± 14)%. Thus, there is a hint of a decrease in disc frequency towards lower masses that could also explain the slightly higher disc frequency determined by Oliveira et al. (2004). However this result is not conclusive and these disc frequencies are entirely consistent with no mass dependence. In particular in the lower mass bin, objects have redder intrinsic colours and with increasing uncertainties in the L′-band photometry, the measurements are less capable of identifying excesses.

It is still not clear whether disc frequencies or disc dissipation time scales are mass dependent. Lada et al. (2000) find high disc frequencies from F to late M spectral types for the 1 Myr-old Trapezium cluster, suggesting that the probability of disc formation around a star is both high and essentially mass independent. However, in their more recent work, Lada et al. (2004) find a hint that the disc frequency around brown dwarfs in the Trapezium cluster might be lower than around stellar objects, but completeness issues make this result inconclusive. For IC 348 (2−3 Myr) Haisch et al. (2001a) suggest a disc frequency decrease from spectral types G down to M. Recently, Lada et al. (2006) analysed Spitzer near- and mid-IR photometry of IC 348 and they find that the disc frequency peaks for late-K to early-M spectral types, suggesting that disc dissipation is mass dependent. The disc frequencies we have determined for the different mass bins are consistent with the IC 348 result but are also statistically consistent with a single disc frequency for the σ Orionis cluster across the mass range. To settle this question in a conclusive way, it would be necessary to gather a larger sample of very low-mass cluster members with better signal-to-noise ratio measurements in the L-band.

5.3 Accretors in the σ Ori cluster

Strong Hα emission and broad line profiles were the classical indicator of young stars with discs, but we now know that they only identify actively accreting discs (e.g., White & Basri 2003; Muzerolle et al. 2003; Barrado y Navascués et al. 2003). In our sample, 33 objects have Hα equivalent width measurements (EW[Hα]) or have been identified as accretors based on the width of the Hα profile (Kenyon et al. 2005) (Table 2 and Fig. 5). Using the White & Basri (2003) criterion of EW[Hα] as a function of spectral type, we can identify stars with a Hα "excess emission", i.e. objects that exhibit emission strong enough to indicate active accretion onto the star — the Barrado y Navascués & Martín (2003) criterion could also be used, yielding the same results. Out of these 33 cluster members, 10 stars have accretion discs; a fraction of (30 ± 10)% consistent with previous results (30−40%, Zapatero Osorio et al. 2002 and (27 ± 7)%, Barrado y Navascués et al. 2003). Of the 10 objects with an accretion disc, 8 objects have 2-σ significant $(K - L')$ disc detections, while 2 fainter objects have $(K - L')$ excesses at a significance level > 1.5-σ (marginal disc detections). Thus, probably all Hα-identified accretors have circumstellar discs indicated by a $(K - L')$ excess. However, 6 objects show a $(K - L')$ excess but no Hα excess emission, i.e. as expected not all objects with discs are actively accreting.

Of the total sample of 87 objects, 11 stars or about (13 ± 4) % show a 2-σ $(H - K_s)$ excess, also considered an accretion indicator (Hillenbrand et al. 1998) — this is consistent with previous determinations, (6 ± 4) % from Oliveira et al. (2002) and 5−12% from Barrado y Navascués et al. (2003). Of the 33 objects with Hα measurements, 5 objects show an excess in the K_s-band. We note that not all objects with $(H - K_s)$ excess show Hα excess emission and vice-versa (Fig. 5), a fact that can be understood in terms of variability, either in the Hα profile (Guenther & Emerson 1997) or in the K_s-band magnitudes (Carpenter et al. 2001).

The comparison of these indicators reinforces the "hierarchy" of disc identifiers. In a sample of young objects with measurements of all three disc indicators: a $(K - L')$ excess identifies most (if not all) circumstellar discs, Hα excess emission identifies those discs actively accreting, while $(H - K)$ excesses identify discs with higher accretion rates, with factors like system geometry and stellar parameters also playing a role (Hillenbrand et al. 1998).

6 SUMMARY

We present new K and L′ observations of PMS stars in the σ Orionis cluster, obtained at UKIRT. We have computed the disc frequency of the cluster using a 2-σ $(K - L')$ excess as the disc indicator. Of the 83 cluster members in the sample, 27 objects have a circumstellar disc, indicating a disc frequency of (33 ± 6)%, consistent with previous determinations (Oliveira et al. 2004). If instead the $JHKL'$ colour-colour diagram is used to identify discs, the disc frequency would be (40 ± 7)%. With an age of 3−5 Myr, this disc frequency is consistent with the 3 Myr disc half-life as determined by Haisch et al. (2001b). As the age of the cluster is uncertain (values between 2.5 Myr and 8 Myr can be found in the literature) we are unable to derive firmer conclusions on the disc dissipation timescale, but an older age for the σ Ori cluster would imply a slower rate of disc dis-

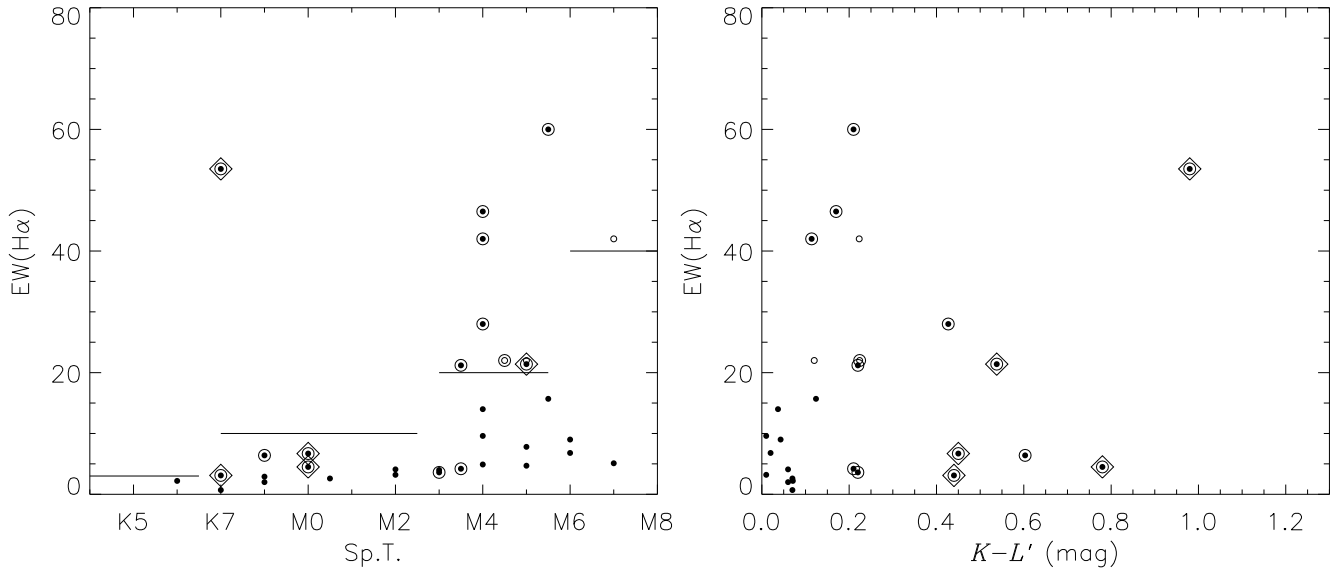

Figure 5. Hα measurements as a function of spectral type and $(K - L')$ colour. Objects either have EW[Hα] measurements in Table 2 (filled circles) or have been identified as accretors based on the line width (Kenyon et al. 2005, open circles). Double-circle objects have 2-σ significant $(K - L')$ excesses while diamonds are objects with 2-σ significant $(H - K_s)$ excesses (see text). The full lines represent the White & Basri (2003) criterion for the identification of accreting cluster members.

persal. We find no evidence of spatial segregation of objects with or without circumstellar discs.

We have investigated a possible mass dependence of the disc frequency. We find that for stars more massive than $0.5\,M_\odot$ the disc frequency is $(42 \pm 13)\%$, decreasing to $(28 \pm 8)\%$ and $(25 \pm 14)\%$ respectively for stars with masses in the range $0.5\,M_\odot > M \geqslant 0.1\,M_\odot$ and $0.1\,M_\odot > M \geqslant 0.04\,M_\odot$. These different disc frequencies are statistically consistent with a single disc frequency across the mass range. On the other hand, it could also hint at a mass dependence of the disc frequency in the same sense as that found by Lada et al. (2006) in IC 348.

For some cluster members in our sample, Hα equivalent width measurements are also available. We investigate the hierarchy of disc indicators and confirm that a $(K - L')$ excess identifies the majority of circumstellar discs, Hα excess emission identifies discs actively accreting, while a $(H - K)$ excess identifies discs with higher accretion rates primarily around the more massive young stars.

ACKNOWLEDGEMENTS

We thank the staff of United Kingdom Infra-Red Telescope (UKIRT) for their support. UKIRT is operated by the Joint Astronomy Centre on behalf of the UK Particle Physics and Astronomy Research Council (PPARC). This publication makes use of data products from the Two Micron All Sky Survey, which is a joint project of the University of Massachusetts and the Infrared Processing and Analysis Center/California Institute of Technology, funded by the National Aeronautics and Space Administration and the National Science Foundation. JMO and MTR acknowledges financial support from PPARC. We thank the referee for useful comments.

REFERENCES

Baraffe I., Chabrier G., Allard F., Hauschildt P., 1998, A&A, 337, 403
Barrado y Navascués D., Béjar V.J.S., Mundt R. et al., 2003, A&A, 404, 171
Barrado y Navascués D., Martín E.L., 2003, AJ, 126, 2997
Béjar V.J.S., Martín E.L., Zapatero Osorio M.R. et al., 2001, ApJ, 556, 830
Bessell M.S., Brett J.M., 1988, PASP, 100, 1134
Brandner W., Zinnecker H., Alcalá J.M. et al., 2000, AJ, 120, 950
Brown A.G.A, de Geus E.J., de Zeeuw P.T., 1994, A&A, 289, 101
Burningham B., Naylor T., Littlefair S.P., Jeffries R.D., 2005, MNRAS, 363, 1389
Caballero J.A., 2005, AN, 326, 1007
Carpenter J.M., 2001, AJ, 121, 2851
Carpenter J.M., Hillenbrand L.A., Skrutskie M.F., 2001, AJ, 121, 3160
Cutri R.M., Skrutskie M.F., Van Dyk S. et al., 2003, Explanatory Supplement to the 2MASS All Sky Data Release
Feigelson E.D., Gaffney J.A. III, Garmire G., Hillenbrand L.A., Townsley L., 2003, ApJ, 584, 911
Franciosini E., Pallavicini R., Sanz-Forcada J., 2005, A&A, 446, 501
Guenther E.W., Emerson J.P., 1997, A&A, 321, 803
Haisch K.E., Lada E.A., Lada C.J., 2000, AJ, 120, 1396
Haisch K.E., Lada E.A., Lada C.J., 2001a, ApJ, 553, 153
Haisch K.E., Lada E.A., Lada C.J., 2001b, AJ, 121, 2065
Hawarden T.G., Leggett S.K., Letawsky M.B. et al., 2001, MNRAS, 325, 563
Hillenbrand L.A., Strom S.E., Calvet N. et al., 1998, AJ, 116, 1816

Jeffries R.D., Evans P.A., Pye J.P., Briggs K.R., 2006, MNRAS accepted, astro-ph/0512441
Kenyon M.J., Jeffries R.D., Naylor T., Oliveira J.M., Maxted P.F.L., 2005, MNRAS, 356, 89
Lada C.J., Muench A.A., Luhman K.L., 2006, AJ in press, astro-ph/0511638
Lada C.J., Muench A.A., Lada E.A., Alves J.F., 2004, AJ, 128, 1254
Lada C.J., Muench A.A., Haisch K.E et al., 2000, AJ, 120, 3162
Lecar M., Sasselov D.D., 2003, ApJ, 596, L99
Leggett S.K., Hawarden T.G., Currie M.J., 2003, MNRAS, 345, 144
Megeath S.T., Hartmann L., Luhman K.L., Fazio G.G., 2005, ApJ, 634, 113
Muzerolle J., Hillenbrand L., Calvet N., Briceño C., Hartmann L., 2003, ApJ, 592, 266
Oliveira J.M., Jeffries R.D., Kenyon M.J., Thompson S.A., Naylor T., 2002, A&A, 382, 22
Oliveira J.M., van Loon J.Th., 2004, A&A, 418, 663
Oliveira J.M., Jeffries R.D., van Loon J.Th., 2004, MNRAS, 347, 1327
Scholz A., Eislöffel J., 2004, A&A, 419, 249
Sherry W.H., Walter F.M., Wolk S.J., 2004, AJ, 128, 2316
Tokunaga A.T., Simons D.A., Vacca W.D., 2002, PASP, 114, 180
van Loon J.Th., Oliveira J.M., 2003, A&A, 405, 33
Uchida K.I., Calvet N., Hartmann L. et al., 2004, ApJS, 154, 439
White R.J., Basri G., 2003, ApJ, 582, 1109
Wolk S.J., 1996, Ph.D. thesis, State Univ. New York at Stony Brook
Wood K., Lada C.J., Bjorkman J.E. et al., 2002, ApJ, 567, 1183
Zapatero Osorio M.R.Z., Béjar V.J.S., Pavlenko Y. et al., 2002, A&A, 384, 937
Zapatero Osorio M.R.Z., Béjar V.J.S., Martín E.L. et al., 2000, Sci, 290, 103

This paper has been typeset from a TEX/ LATEX file prepared by the author.